Accurate Measurements and Error Analysis of Bi_2Te_3-Based Low-Temperature Thermoelectrics

Jie Zhang[1,2], Yixuan Ge[2], Minhua Huang[2], Xiaohan Qin[2], Chao Xin[2], Linhan Wang[2], Wenfeng Du[1,2], Tianbo Lu[2], Huaizhou Zhao[2], Wenjie Liang[2,3,4], Yongjun Cao[1*], and Guodong Li[2*]

[1]*College of Physics and Electronic Information, Inner Mongolia Normal University, Hohhot 011517, China*
[2]*Institute of Physics, Chinese Academy of Sciences, Beijing 100190, China*
[3]*School of Physical Sciences, University of Chinese Academy of Sciences, Beijing 100190, China*
[4]*Songshan Lake Materials Laboratory, Dongguan 523808, China*

(Received 27 March 2025; accepted manuscript online 16 April 2025)

The accurate characterization of thermoelectric properties at low temperatures is crucial for the development of high-performance thermoelectric cooling devices. While measurement errors of thermoelectric properties at temperatures above room temperature have been extensively discussed, there is a lack of standard measurement protocols and error analyses for low-temperature transport properties. In this study, we present a measurement system capable of characterizing all three key thermoelectric parameters, i.e., Seebeck coefficient, electrical conductivity, and thermal conductivity, for a single sample across a temperature range of 10 K to 300 K. We investigated six representative commercial Bi_2Te_3-based samples (three N-type and three P-type). Using an error propagation model, we systematically analyzed the measurement uncertainties of the three intrinsic parameters and the resulting thermoelectric figure of merit. Our findings reveal that measurement uncertainties for both N-type and P-type Bi_2Te_3-based materials can be effectively maintained below 5% in the temperature range of 40 K to 300 K. However, the uncertainties increase to over 10% at lower temperatures, primarily due to the relatively smaller values of electrical resistivity and Seebeck coefficients in this regime. This work establishes foundational data for Bi_2Te_3-based thermoelectric materials and provides a framework for broader investigations of advanced low-temperature thermoelectrics.

DOI: 10.1088/0256-307X/42/5/056304 CSTR: 32039.14.0256-307X.42.5.056304

1. Introduction. Thermoelectric devices (TEDs) utilize the Seebeck effect for power generation and the Peltier effect for heat pumping, enabling direct conversions between heat and electricity in a solid-state form.[1–4] Unlike traditional mechanical energy conversion systems, TEDs offer several advantages, including the absence of moving parts, silent operation, extended service life, and minimal maintenance requirements.[5,6] Thermoelectric cooling devices, in particular, have become essential in various applications such as 5G optical communications,[7,8] medical polymerase chain reactions (PCR),[9–11] and solid-state infrared detectors.[12] This is primarily due to their structural simplicity and compactness.[13,14] Currently, commercial TEDs are predominantly based on Bi_2Te_3-based materials, specifically N-type $Bi_2(Te,Se)_3$ and P-type $(Bi,Sb)_2Te_3$. The performance of these devices is typically evaluated using the dimensionless figure of merit $zT = S^2T/(\rho^*\kappa)$, where S is the Seebeck coefficient, ρ is the electrical resistivity, κ is the thermal conductivity, and T is the absolute temperature.[15,16] Therefore, precise measurements of these temperature-dependent material properties are crucial for advancing TED technology.

There have been a number of studies addressing the characterization techniques and error analysis of Bi_2Te_3-based thermoelectric materials.[17–21] For instance, Borup *et al.*[17] highlighted the influence of sample geometry, temperature measurement, and contact resistance on the electrical measurements, as well as the impact of thermal contact and thermal radiation on the thermal measurements. Starting from 2009, International Energy Agency (IEA) organized international round-robin test to evaluate the thermoelectric transport properties of bulk Bi_2Te_3 materials across seven laboratories.[18,19] The results revealed that the error in calculating the thermoelectric figure of merit (zT) was approximately ±11.7% near room temperature and increased to ±20.9% at 475 K. Wei *et al.*[21] emphasized that repeatability is more critical than accuracy when using commercial instruments for measurements. Their findings indicated that repeatability can be stably controlled within an error range of ±5% when using the same instrument for measurements. Recently, Heremans *et al.*[20] identified the error sources in thermoelectric measurements and noted that the uncertainty in zT above room temperature is of the order 15%–20%. However, most of these studies have focused on measurements at temperatures above room temperature, with limited

*Corresponding author. Email: phyjcao@imnu.edu.cn; gdli@iphy.ac.cn
© 2025 Chinese Physical Society and IOP Publishing Ltd. All rights, including for text and data mining, AI training, and similar technologies, are reserved.

research conducted in the sub-room temperature range. As TEDs find increasing applications in deep cryogenic regions, precise low-temperature transport measurements and proper error analysis of Bi_2Te_3-based thermoelectric materials are becoming increasingly important.

In this study, we present a methodology for characterizing the low-temperature properties of thermoelectric materials. Our approach employs a four-point method for resistivity measurement and a steady-state technique for determining thermal conductivity and the Seebeck coefficient on a single sample. We investigated representative N-type $Bi_2(Te,Se)_3$ and P-type $(Bi,Sb)_2Te_3$ samples sourced from different leading commercial manufacturers, primarily fabricated via zone melting (ZM), spark plasma sintering (SPS), and hot extrusion (HE) techniques. The thermoelectric performance of these materials was systematically evaluated across a temperature range of 10 K to 300 K. Additionally, we conducted a comprehensive analysis of common error sources in low-temperature thermoelectric measurements and quantified the uncertainty in zT during the measurement process. Our results demonstrate that the measurement errors of zT values at 300 K for N-type $Bi_2(Te,Se)_3$ and P-type $(Bi,Sb)_2Te_3$ could be effectively constrained within 2.91% and 2.94%, respectively. From 300 K down to 40 K, the measurement error remains within 5% and slightly increases at lower temperatures.

2. Measurement Setup for Full zT Values of Bulk Samples. The experimental process begins with the preparation of Bi_2Te_3-based thermoelectric materials, which are fabricated via three representative techniques: ZM, SPS, and HE. These materials are carefully shaped into rectangular samples with dimensions approximately 6 mm in length, 2 mm in width, and 1 mm in thickness. This standardized geometry ensures consistency in measurements and minimizes potential variations in sample properties.

The full zT value measurement setup is shown in Fig. 1. The measurement process involves two primary steps. First, the electrical resistivity of the sample is determined using the four-point method. As illustrated in Fig. 1(a) and represented by the actual sample in Fig. 1(c), four electrodes are evenly placed on the sample's surface. Current is applied through the outer two electrodes, while the voltage drop is measured across the inner two electrodes. This configuration helps to reduce contact resistance effects, ensuring accurate resistivity calculations. The resistivity ρ is then derived using the sample's dimensions and the measured resistance R via the formula $\rho = RA/L$, where A is the cross-sectional area and L is the distance between the inner electrodes. It is worth noting that proper electrode materials (silver paste in this work) should be selected to make sure ohmic contacts being established between the electrodes and the Bi_2Te_3-based materials (Fig. S1 in Supplementary Materials).

Subsequently, on the same sample, the Seebeck coefficient S and thermal conductivity κ are measured by using the steady-state method. As shown in Figs. 1(b) and 1(d),

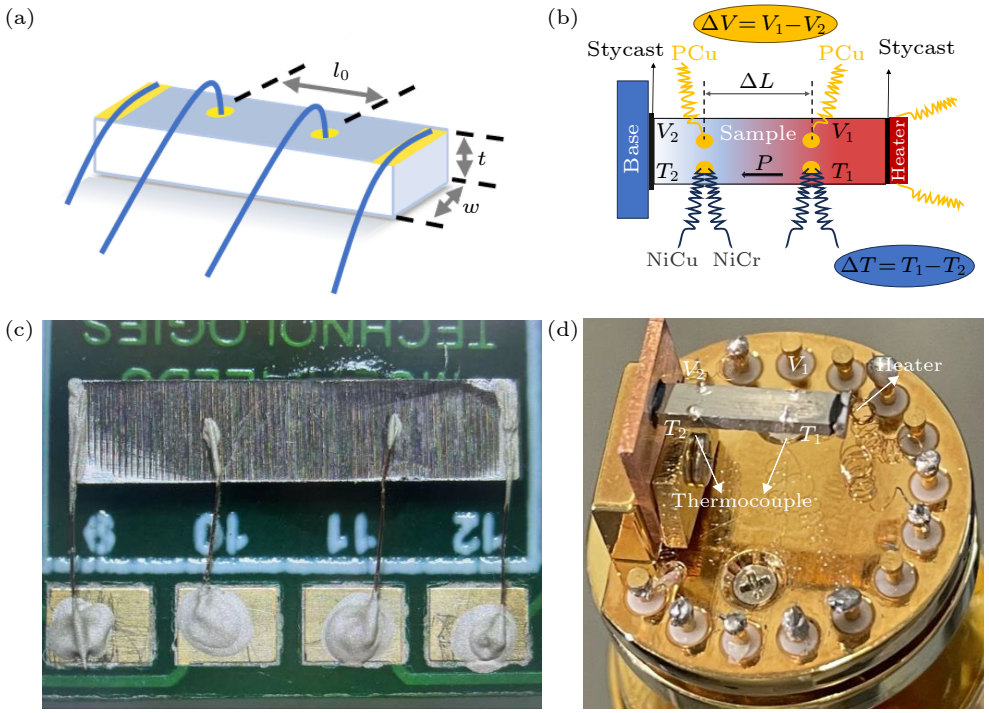

Fig. 1. Thermoelectric transport property measurement setup. (a) Schematic picture for the electrical resistivity ρ measurement, with l_0 being the distance between the centres of the two voltage electrodes, w and t being width and thickness of the sample, respectively. (b) Configuration for thermal conductivity κ and the Seebeck coefficient S, thermocouples mounted on the sample surface monitor the temperature gradient ΔT, while phosphor copper wires measure the induced voltage difference ΔV. (c) Photograph of electrical measurement connections. (d) Photograph of thermal measurement connections.

the sample is securely mounted between a heater and a heat sink using thermally conductive paste (Stycast® in this work) to ensure good thermal contact. When the heater is activated, a stable temperature gradient ΔT is established across the sample. Two sets of thermocouples (E-type in this work) measure the temperatures at two distinct points on the sample, allowing for precise calculation of the temperature difference. Additionally, a pair of phosphorus copper wires measures the potential difference ΔV across the same points. The Seebeck coefficient is then calculated as $S = \Delta V/\Delta T$, while the thermal conductivity is determined using Fourier's Law, $\kappa = q\Delta L/(A\Delta T)$, where q is the heat flux and ΔL is the distance between the thermocouples. When performing thermal conductivity measurements at low temperatures, the thermal radiation effect between the sample and its surrounding environment cannot be neglected. To ensure data accuracy, thermal radiation corrections were applied to the measured thermal conductivity data after the measurements were completed, with the emissivity values of N-type $Bi_2(Te,Se)_3$ and P-type $(Bi,Sb)_2Te_3$ being 0.57 and 0.51, respectively (Fig. S2).

All measurements are conducted within a chamber equipped with a liquid helium compressor (Multifield ColdTube®, China), which can provide a temperature range from 4.2 K to 325 K. For electrical measurements, samples are first glued to a holder by N-grease then loaded in the measurement chamber filled with helium gas, ensuring good thermal contact and minimal environmental interference. For thermal measurements, a copper shield cover is screwed outside of the sample and pumped to high vacuum, which could effectively minimize the sample heat loss from thermal convection and radiation. The measurements are performed every 20 K automatically and for each temperature point we wait long enough to ensure the sample reaches thermal equilibrium. Electrical measurements are made by inputting an AC signal through a Keithley 6221, which is combined with a voltage amplifier SR560 and a lock-in amplifier SR830 to collect the voltage signals.

3. Low-Temperature Thermoelectric Properties of N-Type $Bi_2(Te,Se)_3$. Currently, commercially available N-type $Bi_2(Te,Se)_3$ thermoelectric materials are primarily fabricated using two distinct techniques: ZM[22] and HE.[23] Generally, ZM samples exhibit superior thermoelectric performance, albeit with poor mechanical robustness.[24] In contrast, HE samples demonstrate enhanced mechanical properties, albeit at the expense of slightly diminished thermoelectric efficiency. For this investigation, we selected one ZM sample and two HE samples from different manufacturers, named as N-ZM, N-HE-1, and N-HE-2, respectively. The temperature-dependent resistivity, Seebeck coefficient, thermal conductivity, and power factor of these samples are comprehensively summarized in Fig. 2.

Figure 2(a) illustrates the temperature dependence of electrical resistivity for all three types of samples. As the temperature increases, the electrical resistivity increases monotonically, indicating that all $Bi_2(Te,Se)_3$ samples are degenerately doped and showed metallic ρ-T behavior. At 300 K, the electrical resistivity of the N-type $Bi_2(Te,Se)_3$ samples ranges from 7 to 11 μΩ·m, depending on the sample fabrication technique. The Seebeck coefficient for all three samples, as shown in Fig. 2(b), exhibits a consistent increase with rising temperature. Compared to the HE samples, the ZM sample demonstrates particularly higher

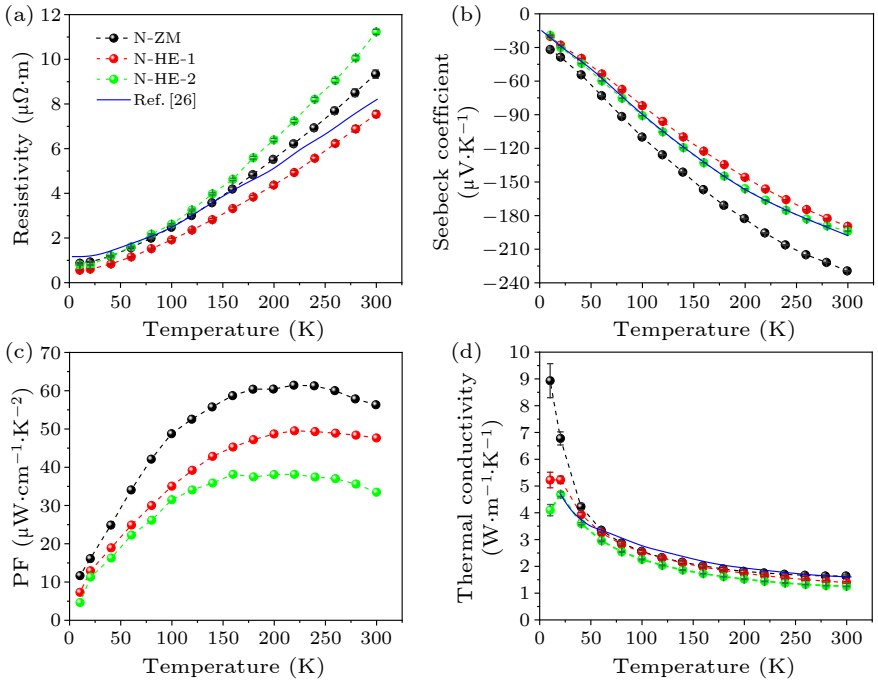

Fig. 2. Thermoelectric properties and measurement uncertainty of commercial N-type $Bi_2(Te,Se)_3$ at low temperatures. (a) Electrical resistivity. (b) Seebeck coefficient. (c) Power factor. (d) Thermal conductivity. The dashed lines in the figures serve as guides for the eye.

Seebeck values across the entire temperature range. The power factor is calculated using the formula $PF = S^2/\rho$, and its temperature dependence is presented in Fig. 2(c). As the temperature increases, the PF values for all three samples initially increase and then decrease, with peak values occurring between 200–250 K. Notably, the ZM sample achieves the highest PF values among the three types of samples.

The temperature-dependent thermal conductivity for all three N-type samples is presented in Fig. 2(d). Compared to the HE samples, the ZM samples exhibit a better crystalline quality, resulting in slightly higher thermal conductivity across the entire measured temperature range. All three samples display similar temperature-dependent behavior, with a peak thermal conductivity observed between 10 K–20 K. At higher temperatures, the thermal conductivity decreases as Umklapp scattering (phonon-phonon interactions) becomes more dominant.[25] For comparison, one set of low-temperature thermoelectric transport data reported by Mao *et al.*[26] is also referred in the figures, as shown by the blue lines.

4. Low-Temperature Thermoelectric Properties of P-Type $(Bi,Sb)_2Te_3$. At present, three primary techniques dominate the commercial production of P-type $(Bi,Sb)_2Te_3$ thermoelectric materials: ZM,[27,28] SPS,[29,30] and HE.[31] In this study, we selected representative samples from each fabrication method, named as P-ZM, P-SPS, and P-HE. The variations in electrical resistivity, Seebeck coefficient, thermal conductivity, and power factor as a function of temperature for these samples are presented in Fig. 3.

As shown in Figs. 3(a) and 3(b), similar to N-type $Bi_2(Te,Se)_3$, both the resistivity and Seebeck coefficient of P-type $(Bi,Sb)_2Te_3$ display a steady increase with rising temperature. At 300 K, the electrical resistivity of the P-type $(Bi,Sb)_2Te_3$ samples ranges from 7 to 12 μΩ·m, with specific values varying depending on the fabrication methods employed for each sample. Among the three samples investigated, the HE sample exhibits the highest values for both resistivity and Seebeck coefficient, followed by the ZM sample and then the SPS sample. Interestingly, the power factor values of the three samples demonstrate surprisingly consistent behavior. As shown in Fig. 3(c), the power factor values of all three samples initially increase with rising temperature, reaching a peak in the temperature range of 200–220 K, and then gradually decrease thereafter.

As shown in Fig. 3(d), the thermal conductivity of all three types of P-type $(Bi,Sb)_2Te_3$ samples initially increases and then decreases with temperature. Similar to that of N-type $Bi_2(Te,Se)_3$ samples, the P-type ZM sample exhibits the highest thermal conductivity across the entire temperature range, attributed to its high crystallinity. The SPS sample displays the lowest thermal conductivity below 80 K, likely due to enhanced phonon scattering caused by grain boundaries and defects introduced during the sintering process.[29] Above 80 K, the HE sample exhibits the lowest thermal conductivity, reaching a minimum value of 1.10 $W \cdot m^{-1} \cdot K^{-1}$ at 300 K.

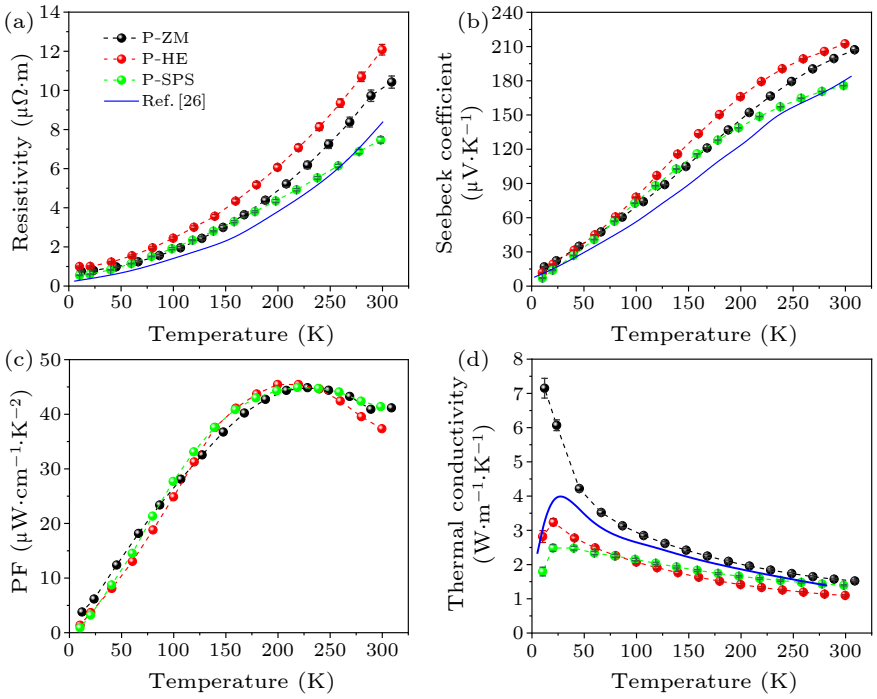

Fig. 3. Thermoelectric properties and measurement uncertainty of commercial P-type $(Bi,Sb)_2Te_3$ at low temperatures. (a) Electrical resistivity. (b) Seebeck coefficient. (c) Power factor. (d) Thermal conductivity. The dashed lines in the figure serve as guides for the eye.

5. zT of N-Type and P-Type Bi_2Te_3-Based Thermoelectric Materials. The zT values of N-type $Bi_2(Te,Se)_3$ and P-type $(Bi,Sb)_2Te_3$ materials, calculated using the formula $zT = S^2T/\rho\kappa$, are presented in Fig. 4. As shown in Fig. 4(a), the zT values of all N-type $Bi_2(Te,Se)_3$ samples show a consistent upward trend with rising temperature. Among these, the ZM sample demonstrates the most remarkable performance, achieving zT value of 1.03 at 300 K. While the two HE samples have been reported to possess better mechanical properties than the ZM samples, they exhibit slightly lower zT values. This might be attributed to high-density grain boundaries and defects,[32] which reduce thermal conductivity on one hand but also impair electrical transport on the other hand.

Similarly, the temperature-dependent zT values of P-type $(Bi,Sb)_2Te_3$ samples are shown in Fig. 4(b). Since the power factors of the three samples are very similar, thermal conductivity becomes the dominant factor influencing zT. Among the samples, the HE sample exhibits the lowest thermal conductivity, particularly above 80 K. Consequently, unlike the N-type $Bi_2(Te,Se)_3$ materials, the P-type HE sample achieves superior zT values compared to the SPS and ZM samples, reaching zT value of 1.02 at 300 K.

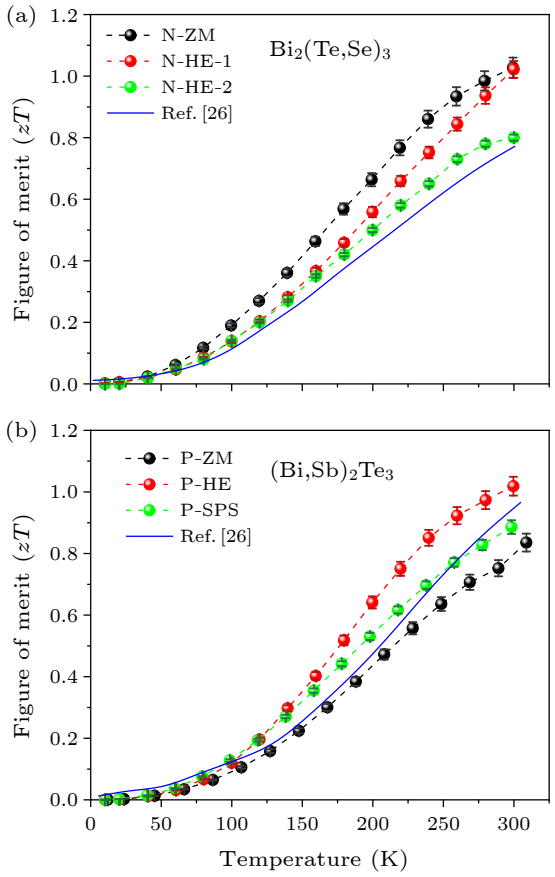

Fig. 4. Low-temperature thermoelectric figure of merit zT as a function of temperature and its uncertainty. (a) Commercial N-type $Bi_2(Te,Se)_3$. (b) Commercial P-type $(Bi,Sb)_2Te_3$. The dashed lines in the figure serve as guides for the eye.

6. Error Analysis of zT. In the framework of error propagation, the error of zT can be expressed as following (Supplementary Materials):

$$\Delta(zT) = \sqrt{\left(\frac{2ST}{\rho\kappa}\Delta S\right)^2 + \left(-\frac{S^2T}{\rho^2\kappa}\Delta\rho\right)^2 + \left(-\frac{S^2T}{\rho\kappa^2}\Delta\kappa\right)^2}. \tag{1}$$

Simplification yields the following expression:

$$\Delta(zT) = \frac{S^2T}{\rho\kappa}\sqrt{\left(\frac{2\Delta S}{S}\right)^2 + \left(\frac{\Delta\rho}{\rho}\right)^2 + \left(\frac{\Delta\kappa}{\kappa}\right)^2}. \tag{2}$$

Thus, the error in zT arises from measurement uncertainties of Seebeck coefficient, electrical resistivity, thermal conductivity. The main sources of error in resistivity include sample geometric dimension errors (such as cross-sectional area A and electrode spacing l_0) and resistance measurement errors (such as instrument resolution and accuracy). Based on these error sources, the error propagation formula for resistivity can be written as

$$\Delta\rho = \rho\sqrt{\left(\frac{\Delta R}{R}\right)^2 + \left(\frac{\Delta A}{A}\right)^2 + \left(\frac{\Delta l_0}{l}\right)^2}. \tag{3}$$

The uncertainty in the Seebeck coefficient S mainly stems from the measurement errors of the voltage difference ΔV and temperature difference ΔT. Voltage measurement errors typically arise from instrument noise and resolution limits, while temperature measurement errors are influenced by sensor accuracy and environmental fluctuations. Based on these factors, the error propagation of the Seebeck coefficient can be described as follows:

$$\Delta S = S\sqrt{\left(\frac{\delta(\Delta V)}{\Delta V}\right)^2 + \left(\frac{\delta(\Delta T)}{\Delta T}\right)^2}. \tag{4}$$

For the thermal conductivity κ, its measurement uncertainty is mainly attributed to the temperature difference ΔT and the uncertainties in the geometric parameters of the sample. In particular, the measurement accuracy of the distance between the two thermocouples ΔL and the cross-sectional area A plays a crucial role in error propagation. The error propagation formula for thermal conductivity is given by,

$$\Delta\kappa = \kappa\sqrt{\left(\frac{\delta(\Delta T)}{\Delta T}\right)^2 + \left(\frac{\Delta A}{A}\right)^2 + \left(\frac{\delta(\Delta L)}{\Delta L}\right)^2}. \tag{5}$$

Therefore, by combining the Eqs. (2)–(5), we could literally calculate zT measurement errors of all the investigated samples. In the following, we take N-type ZM $Bi_2(Te,Se)_3$ and P-type HE $(Bi,Sb)_2Te_3$ as examples. At 300 K, the N-type $Bi_2(Te,Se)_3$ sample demonstrated a resistivity of $9.34 \pm 0.19\,\mu\Omega\cdot$m, with a relative error of 2.03%. Its Seebeck coefficient was measured at $-229.32 \pm 0.03\,\mu$V/K, with a quite low relative error of 0.01%. The thermal conductivity was found to be $1.64 \pm 0.04\,$W/m·K, with a relative error of 2.44%. By propagating these errors, the thermoelectric figure of merit was calculated to be 1.03 ± 0.03, with a relative error of 2.91%. For the P-type HE $(Bi,Sb)_2Te_3$ sample, the corresponding values are $12.08 \pm 0.27\,\mu\Omega\cdot$m for the resistivity, $212.40 \pm 0.03\,\mu$V/K for the Seebeck coefficient, and

1.10 ± 0.02 W/m·K for the thermal conductivity, with relative errors of 2.24%, 0.01%, and 1.82%, respectively. The calculated zT value is 1.02, with an uncertainty of 0.03, which corresponds to a relative error of 2.94%.

Following the above rules, zT errors for all the samples are calculated in the whole low temperature range, as shown in Fig. 4. For all three types of N-type samples, the relative measurement uncertainty remains within 4% across the temperature 40 K to 300 K, with the HE samples exhibiting the smallest deviation ($< 2\%$), mainly due to smaller measurement errors at different positions, which reduces the overall uncertainty. In contrast, the uncertainties of all three kinds of P-type samples show similar magnitudes over the whole measured temperature range. Compared to N-type $Bi_2(Te,Se)_3$, P-type $(Bi,Sb)_2Te_3$ samples exhibit slightly larger errors but remain below 5%. However, at 10 K, the measurement errors for both N-type $Bi_2(Te,Se)_3$ and P-type $(Bi,Sb)_2Te_3$ samples increase to approximately 8%–14%. This is due to the reduction in resistivity and Seebeck coefficient at lower temperatures, which weakens the signal and consequently leads to higher measurement uncertainty.

It is worth noting that the low-temperature zT errors reported in this work are remarkably smaller than those commonly found in conventional knowledge, which typically range around 20%. This significant improvement can be attributed to several key aspects of our experimental approach: (1) ensuring the reliability of measurements by preparing all samples in a standard geometry; (2) establishing good ohmic contacts for both resistivity and Seebeck coefficient measurements, effectively eliminating potential influences from contact and thermal potentials; (3) employing a steady-state method to directly measure thermal conductivity, which involves only measuring heat flux and temperature differences, thereby avoiding the need to separately measure thermal diffusivity, density, and specific heat capacity as required in traditional high-temperature thermal conductivity measurements;[33,34] (4) utilizing thin and long wires, such as 25-μm-thick thermocouples and phosphor bronze wires, to connect the sample, thereby minimizing heat loss; (5) employing a well-established and highly stable low-temperature cooling system, featuring high temperature control resolution and excellent stability, effectively ensuring the accuracy of the measurement results; and (6) conducting all measurements on the same sample, which minimizes differences and uncertainties between samples. Furthermore, to ensure the reliability of our results, we performed consistency tests by continuously measuring two samples cut from the same commercial ingots (The N-type ingot was prepared by the HE method, and the P-type ingot by the SPS method). The measurement results exhibited high consistency, further confirming the high reliability and robust credibility of our experimental findings (Figs. S5–S7). For the reader's reference, we provide a set of low-temperature thermoelectric transport data for ZM N-type $Bi_2(Te,Se)_3$ and HE P-type $(Bi,Sb)_2Te_3$ in Section 9 of Supplementary Materials.

7. *Conclusion.* In this study, we systematically investigated the low-temperature (10–300 K) thermoelectric figure of merit zT values and associated measurement uncertainties for various representative commercial N-type and P-type Bi_2Te_3-based materials. Notably, compared to the larger errors commonly encountered in high-temperature measurements, our low-temperature experiments demonstrated exceptional accuracy and stability, representing a significant advancement in the field. For both N-type and P-type Bi_2Te_3-based materials, the zT measurement uncertainties were consistently maintained with a maximum deviation of 5%. This research not only establishes a reliable database for the development of advanced thermoelectric cooling devices, but also lays a robust foundation for further research and applications of low-temperature thermoelectric materials.

Acknowledgements. This work was supported by the National Natural Science Foundation of China (Grant No. 52172259), the National Key Research and Development Program of China (Grant Nos. 2021YFA0718700 and 2022YFB3803900). We thank the Fundamental Research Funds for the Inner Mongolia Normal University (Grant No. 2022JBTD008). We would like to appreciate Prof. Xi'an Fan from Wuhan University of Science and Technology and Zongxiang Kan from Xianghe Oriental Electronic for valuable discussions. This work is partly supported by the Research Platform of Material Genome and the Synergic Extreme Condition User Facility in Huairou, Beijing, China.

References

[1] Snyder G J and Toberer E S 2008 *Nat. Mater.* **7** 105
[2] Zhang X and Zhao L D 2015 *J. Mater.* **1** 92
[3] Ren J 2023 *Chin. Phys. Lett.* **40** 090501
[4] Tritt T M 2011 *Annu. Rev. Mater. Res.* **41** 433
[5] Zhao D and Tan G 2014 *Appl. Therm. Eng.* **66** 15
[6] Redouane N 2023 *Chin. Phys. B* **32** 057307
[7] Han Z, Li J W, Jiang F, Xia J, Zhang B P, Li J F, and Liu W 2022 *J. Mater.* **8** 427
[8] Qiu J H, Yan Y G, Luo T T, Tang K C, Yao L, Zhang J, Zhang M, Su X L, Tan G J, Xie H Y, Kanatzidis M G, Uher C, and Tang X F 2019 *Energy Environ. Sci.* **12** 3106
[9] Wu D and Wu W M 2019 *Sensors* **19** 1609
[10] Bell L E 2008 *Science* **321** 1457
[11] Li G D, Garcia Fernandez J, Lara Ramos D A, Barati V, Pérez N, Soldatov I, Reith H, Schierning G, and Nielsch K 2018 *Nat. Electron.* **1** 555
[12] Meng F K, Zhou L, Song C, and Zhang J P 2025 *Appl. Therm. Eng.* **266** 125457
[13] Liu Q L, Li G D, Zhu H T, and Zhao H Z 2022 *Chin. Phys. B* **31** 047204
[14] Twaha S, Zhu J, Yan Y Y, and Li B 2016 *Renew. Sustain. Energy Rev.* **65** 698
[15] Zhao L D, Dravid V P, and Kanatzidis M G 2014 *Energy Environ. Sci.* **7** 251
[16] Heremans J P, Wiendlocha B, and Chamoire A M 2012 *Energy Environ. Sci.* **5** 5510
[17] Borup K A, De Boor J, Wang H, Drymiotis F, Gascoin F, Shi X, Chen L D, Fedorov M I, Müller E, Iversen B B, and Snyder G J 2015 *Energy Environ. Sci.* **8** 423

[18] Wang H, Porter W D, Böttner H, König J, Chen L D, Bai S Q, Tritt T M, Mayolet A, Senawiratne J, Smith C, Harris F, Gilbert P, Sharp J, Lo J, Kleinke H, and Kiss L 2013 *J. Electron. Mater.* **42** 654
[19] Wang H, Porter W D, Böttner H, König J, Chen L D, Bai S Q, Tritt T M, Mayolet A, Senawiratne J, Smith C, Harris F, Gilbert P, Sharp J, Lo J, Kleinke H, and Kiss L 2013 *J. Electron. Mater.* **42** 1073
[20] Heremans J P and Martin J 2024 *Nat. Mater.* **23** 18
[21] Wei T R, Guan M J, Yu J J, Zhu T J, Chen L D, and Shi X 2018 *Joule* **2** 2183
[22] Shtern M Y, Matyna L I, Rogachev M S, and Merlyan A P 2021 *Proc. IEEE Conf. Russ.* 2481
[23] Lu T B, Wang B Y, Li G D, Yang J W, Zhang X F, Chen N, Liu T H, Yang R G, Niu P J, Kan Z X, Zhu H T, and Zhao H Z 2023 *Mater. Today Phys.* **32** 101035
[24] Zheng G, Su X L, Liang T, Lu Q B, Yan Y G, Uher C, and Tang X F 2015 *J. Mater. Chem. A* **3** 6603
[25] Zhang Y S 2016 *J. Mater.* **2** 237
[26] Mao J, Zhu H T, Ding Z W, Liu Z H, Gamage G A, Chen G, and Ren Z F 2019 *Science* **365** 495
[27] Xu Z J, Hu L P, Ying P J, Zhao X B, and Zhu T J 2015 *Acta Mater.* **84** 385
[28] Zheng Y, Xie H Y, Shu S C, Yan Y G, Li H, and Tang X F 2014 *J. Electron. Mater.* **43** 2017
[29] Pan Y, Wei T R, Cao Q, and Li J F 2015 *Mater. Sci. Eng. B* **197** 75
[30] Bulat L P, Drabkin I A, Karatayev V V, Osvenskii V B, Parkhomenko Y N, Pshenay-Severin D A, and Sorokin A I 2014 *J. Electron. Mater.* **43** 2121
[31] Lavrentev M G, Osvenskii V B, Parkhomenko Y N, Pivovarov G I, Sorokin A I, Bulat L P, Kim H S, Witting I T, Snyder G J, Bublik V T, and Tabachkova N Y 2016 *APL Mater.* **4** 104807
[32] Li Y Z, Liu F, Ying B Y, Liu J Y, He Y Z, Liu K, Li A R, Wu Y Q, Tang Z F, Nan P F, Ge B H, Fu C G, and Zhu T J 2024 *Mater. Today Phys.* **49** 101591
[33] Zhao D L, Qian X, Gu X K, Jajja S A, and Yang R 2016 *J. Electron. Packag.* **138** 040802
[34] Wu M, Shi R C, Qi R S, Li Y H, Feng T, Liu B Y, Yan J Y, Li X M, Liu Z T, Wang T, Wei T B, Liu Z Q, Du J L, Chen J, and Gao P 2023 *Chin. Phys. Lett.* **40** 036801